FISEVIER

Contents lists available at ScienceDirect

Journal of Magnetism and Magnetic Materials

journal homepage: www.elsevier.com/locate/jmmm



Research articles

A low-cost vibrating sample magnetometry based on audio components

Babu R. Sankhi, Emrah Turgut*

Department of Physics, Oklahoma State University, Stillwater OK 74078-3072, USA



ARTICLE INFO

Keywords: Vibrating sample magnetometry Sound-card based instrument Magnetic thin-film

ABSTRACT

In this paper, we developed a low-cost, highly sensitive magnetization characterization instrument using a sound card and compared its sensitivity with commercially available measurement techniques. Firstly, we use an RLC circuit to measure the frequency-dependent response of the sound card and compare it with a lock-in amplifier. Then, we construct a simple but versatile measuring instrument, vibrating sample magnetometer (VSM) based on audio components, where data acquisition is performed by the sound card and the commercial lock-in amplifier. We test our magnetometry by measuring the magnetic hysteresis of three distinct samples: Nickel bulk piece, perm-alloy thin film with an easy-plane anisotropy, and Co/Pt multilayer with perpendicular magnetic anisotropy. We also analyze the magnetizations of three samples for different vibration frequencies and compare the sensitivities of two data acquisition methods. Although the sound card performs slightly worse than the lock-in amplifier at the vibration frequencies lower than 20 Hz due to the frequency cut-off, the sound card provides approximately seven times better sensitivity than the lock-in amplifier does at higher frequencies up to 60 Hz. We found that the sound card based VSM can have a sensitivity as high as 2 micro-emu at 34.7 Hz vibration frequency, which can be suitable for various laboratory and industrial applications.

1. Introduction

Measurement of magnetization is an important characterization step for magnetic materials in the field of condensed matter physics to understand their fundamental properties and to utilize in industrial applications [1]. To quantitatively define the magnetic state of the matter, the induction from the total magnetic moment is usually measured as a function of an external magnetic field, which is known as a magnetic hysteresis measurement [2]. In this method, a hysteresis measurement can provide information about magnetic properties such as retentivity, coercivity, and susceptibility, all of which play crucial roles in studies of magnetic materials [1,3–6]. The most common instruments employing the induction method are SQUID and vibrating sample or coil magnetometries. Although SQUID provides the highest sensitivity ($\sim 10^{-8}$ emu [7]) among three, its operation is costly due to the usage of cryogenic liquids. On the other hand, vibrating sample or coil magnetometers are relatively cost-effective for magnetic hysteresis measurements, and they provide a sensitivity at the order of 10^{-7} emu [6]. Vibrating sample magnetometry (VSM) is more straightforward and sensitive compared to vibrating coil magnetometry; however, the later makes the measurements possible even at sub-Kelvin temperatures [8].

The VSM technique employs a vibrator (e.g., motor) to create a magnetic flux change around the magnetic sample, which induces an

AC emf on pickup coils near the sample. This AC voltage is proportional to the magnetization of the sample, and its measurement can be performed by a dedicated circuit or a lock-in amplifier [9,10]. Although lock-in amplifiers are common in research laboratories for phase-sensitive measurement of modulated signals, they still cost around \$5000. On the other hand, commercially available sound cards are able to record modulating waveforms and provide an extremely high bit analog-to-digital conversion (ADC), similar noise levels to a lock-in amplifier, multiple inputs for synchronous measurements, and default computer interface [11], and these sound cards are widely available at a fifty-times lower price compared to a lock-in amplifier. These advantages make them an alternative for measurements within the frequency range of human hearing, which is between 20 Hz and 20,000 Hz frequencies. Indeed, this frequency range is suitable for many laboratory measurements, such as VSM [12].

In this paper, we evaluated the performance of a 4-channel Behringer (Model UMC404HD) sound card with a 24-Bit ADC resolution and a 192 kHz sampling rate as an alternative to a commercial lock-in amplifier (Signal Recovery 7230) with a 10-Bit ADC resolution. Although a computer can directly acquire the phase sensitive measurements from the lock-in amplifier, we developed a LabView code to compute the in-phase and out-of-phase component of the measured waveform from the sound card. First, we constructed an RLC circuit and

E-mail address: emrah.turgut@okstate.edu (E. Turgut).

^{*} Corresponding author.

measured the frequency-dependent voltage on the resistance by both the sound card and the lock-in amplifier. This RLC circuit test allows us to understand the internal mechanisms, limitations, and advantages of the sound card. Next, we constructed a vibrating sample magnetometer based on audio components, which makes magnetization characterization significantly economical and versatile. In our hysteresis tests, we used three distinct samples: a Nickel piece, a perm-alloy thin film with an easy-plane anisotropy, and a Co/Pt multilayer with perpendicular magnetic anisotropy. All the hysteresis curves of the samples have been successfully obtained, and the Anomalous Hall effect measurement confirms the Co/Pt multilayer hysteresis as being the most challenging sample among three. We also varied vibration frequency to optimize the sensitivity, which is found at the order of 5.4×10^{-6} emu at 34.7 Hz with the sound card and approximately seven times higher compared to the sensitivity of the lock-in amplifier.

We organize the paper as follows: The second section describes the RLC circuit and the LabView code for the phase-sensitive detection with the sound card. The third section details the VSM design, the theoretical calculation of the VSM sensitivity, and the hysteresis characterization of three samples. The fourth section summaries our findings.

2. RLC circuit

An RLC circuit is a common method to evaluate a frequency response of a phase-sensitive measurement by analyzing the amplitude and the phase of an AC voltage from the components. One RLC circuit was already used to evaluate the frequency response of a sound card by comparing a commercial lock-in amplifier [13]. This characterization is a crucial step before using sound cards for scientific purposes, because each sound card may have a different filtering and frequency-dependent amplification, which requires to be determined for calibration purposes. In our RLC circuit, we connected the circuit components in series and attached the measurement units, as in Fig. 1. We employed the oscillator output of the lock-in amplifier as an AC voltage source for the circuit. We also connected this output into Channel 2 input of the sound card to demodulate the signal, which is similar to the reference input in the lock-in amplifier. The voltage dropped across the resistor is first measured by the lock-in amplifier and then by the sound card, both of which are analyzed by Labview codes. We avoided simultaneous measurements by two instruments to prevent any cross-talk. Below we give a background about the phase-sensitive measurement of the modulated signal, which will be helpful to elaborate our home-made lock-in code in LabVIEW software.

The voltage on the resistor R (V_R), can be written as [13];

Fig. 1. Schematic of the RLC-circuit and connections with the lock-in amplifier and the sound card. The frequency-dependent voltage on R (V_R) is measured by the lock-in amplifier and the sound card.

where V_0 , f, L, and C are the amplitude and frequency of the sinusoidal input, inductance, and capacitance of circuit elements, respectively. The resonance frequency is simply $f_0 = \{2\pi (LC)^{1/2}\}^{-1}$. The phase difference between the input signal and the V_R is

$$\delta = Arctan\left[\left(2\pi fL - \frac{1}{2\pi fC}\right)R^{-1}\right] \tag{2}$$

In a phase-sensitive detection, a signal $V_s = A_s \sin(2\pi ft + \delta)$ is mixed with both in-phase reference $\sin(2\pi ft)$ and out-of-phase reference $\cos(2\pi ft)$ signals. After mixing, the resulting voltages would be $X = \frac{A_s}{2} \cos\delta + AC$ for the in-phase reference and $Y = \frac{A_s}{2} \sin\delta + AC$ for the out-of-phase reference. By using a low-pass filter, we filter the AC components and only retain the DC components of X and Y signals, which can be directly read from our lock-in amplifier. Then, the amplitude and the phase on R are calculated by $A_s = |X + iY|$ and $\delta = \text{Angle } [X + iY]$, where Angle is a function to find the angle of the complex number

While commercial lock-in amplifiers can straightforwardly provide X and Y components of the signal, we implemented additional data processing after we acquire the signal V_s and the reference using the sound card. Fortunately, these processes are relatively fast and straightforward by today's personal computers and widely available software.

In Fig. 2, we show the block diagram of the phase-sensitive detection process, which is implemented by LabView software. The signal and the reference waveforms are measured by Channel 1 and Channel 2 inputs of the sound card, respectively, at 24-Bit ADC and 192 kHz sampling rate. Because the reference signal is strong enough (0.1 Volt), the first part of the code called VI-1 accurately calculates the frequency, amplitude, and phase of the reference signal. To find the out-of-phase reference, we apply a 90-degree phase shift to the reference in the second part of the code called VI-2 using the sampling info from VI-1. Next, we mix the input signal with both in-phase and out-of-phase reference signals resulting in the two outputs, i.e. X and Y. By using Butterworth low-pass filter, we reject the AC component and finally obtain the DC components of X and Y values. This filter function also uses the vibration frequency obtained from the VI-1 and valid high and low-frequency cut-offs [14].

In our RLC experiment, we first measure X and Y components with the lock-in amplifier and then repeat the measurement with the sound card by varying the frequency of the input signal between 5 Hz and 50 kHz. The circuit elements used in the circuit are resistance (R), inductance (L), and capacitance (C) with the values of 5.0 Ω , 116.8 mH, and 1.0 μ F, respectively. The measured frequency-dependent amplitudes and phases from the sound card and lock-in amplifier are plotted in Fig. 3(a) and (b), respectively. Fig. 3(a) shows a perfect agreement between the sound card and lock-in for the amplitude of the signal. However, in Fig. 3(b) the sound card shows small discrepancies for the phases below 20 Hz and above 3 kHz frequencies. Our theoretical calculations obtained by Eqs. (1) and (2) and shown by the black curves in Fig. 3 mostly agree with the experimental findings, yet the quality factor is different due to the non-ideal inductance and capacitance in the circuit.

Notably, the sound card shows a limitation for low frequencies, e.g. below 20 Hz. This originates from high-pass filters used in most of the sound cards due to our hearing limit below 20 Hz. Our sound card still can measure the amplitude correctly, but the phase has an approximately 10% error below 15 Hz. Secondly, other abnormalities at the high frequencies in Fig. 3(b) originate from the digitalization of the signal and the reference and relative delay between them, which becomes significant at high frequencies after 2 kHz. By using an RLC circuit, we conclude that the sound card has comparable specifications between 20 Hz and 2 kHz and measurements below 20 Hz and above 2 kHz frequencies require additional precaution. Next, we implement our sound card as a magnetometry measurement instrument to

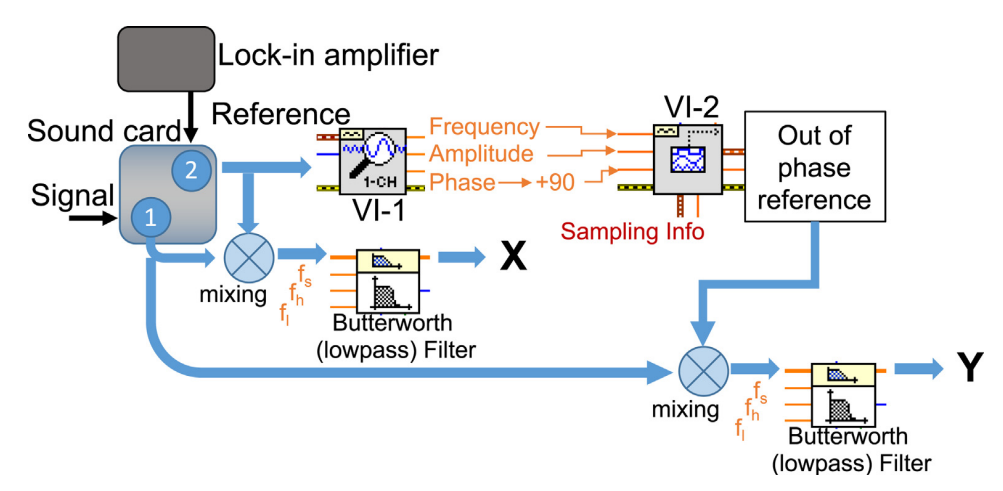


Fig. 2. Diagram of the LabView code for the detection of phase-sensitive signals with the sound-card. The sound card acquires the signal (V_R) from the resistor and the reference from the lock-in amplifier. Next, VI-1 calculates the frequency, amplitude, and phase of the reference, and VI-2 produces the out-of-phase reference. These two in-phase and out-of-phase references are mixed with the signal and we apply a Butterworth filtering to find the DC components, which are referred as X and Y signals.

characterize three specific magnetic materials.

3. Vibrating sample magnetometer

In our VSM design (Fig. 4), we use a woofer speaker and an audio amplifier as the vibrator, exploiting the availability of commercial audio components. The speaker oscillates the sample and creates sinusoidal magnetic induction, which is then picked up by the pick-up coils. For the pick-up coils, choosing the most sensitive coil configuration is a tedious task, and there is already a significant amount of literature on this topic. Mallison et al. used a 4-coil configuration based on the reciprocity theorem [15], which employs a symmetric arrangement for simplicity. Besides, Bernards [16] had studied 8-coil and 12coil configurations and stated the superiority of later one as the output signals were primarily affected by the image charges in the 8 coil configuration [16,17]. For complicated arrangements of the coils, Zieba et al. presented an approximate solution of sensitivity function by using spherical harmonic expansion [18]. In addition to previous works, there are recent studies to improve sensitivity and the data acquisition and process in the VSM technique as being an important characterization instrument [19-23].

In our VSM, we used the 4-coil configuration as Mallison et al. described [15] to have a high sensitivity while keeping the setup compact and simple. The axes of the coils are parallel to the applied magnetic field with an electromagnet, which is along the z-axis. Even though this configuration allows us to measure the magnetization in only one direction, using more coils and sensing magnetization in multiple directions is left as a future study. As illustrated in Fig. 4, along the z-axis, the electromagnet creates a uniform magnetic field that is recorded by a

Gaussmeter, and the sample is vibrated along the x-axis. As the magnetic field is swept between two saturated states, serially connected pick-up coils pick up the periodic flux change. Resulting sinusoidal voltage is sensitively measured by the lock-in amplifier and the sound card turn by turn.

Next, we describe the experimental parameters, which are used to calculate the induced voltage on the pick-up coils. An individual coil has an outer radius ${\bf r}_2=8.93$ mm, an inner radius ${\bf r}_1=4.22$ mm, and a width of ${\bf w}=8.74$ mm. We use AWG 42 copper magnet wire with a diameter of D = 0.07112 mm to wrap the pick-up coils. The number of turns of each coil is calculated by $n=\frac{(r_2-r_1)w}{D^2}$ and found to be 8118. The external magnetic field acts along the z-direction and we take the sample as a point dipole m. The z component of the magnetic field (B_z) due to the magnetization (m) is

$$B_Z = \mu_0 m (3z^2 - x^2 - y^2 - z_0^2) \left(4\pi (x^2 + y^2 + z_0^2)^{\frac{5}{2}} \right)^{-1}$$
 (3)

where μ_0 is the magnetic permeability of a vacuum. The coils are fixed on a 3D printed frame, which keeps z_0 constant at 13.24 mm. The coils are also 25 mm apart in the x-direction. The flux produced on a coil is found by $\phi_z = \iint B_Z dx dy$, where we change variables to the cylindrical coordinate of a coil by $x = x_0 + \rho sin\theta$ and $y = \rho cos\theta$. We then express the integral by $\theta = 0 \rightarrow 2\pi$ and $\rho = 0 \rightarrow r_i$ limits, where r_i is the radius of the ith wrap along the radius. There are approximately 66 layers $((r_2 - r_i)/D)$ along the radius and 123 layers (w/D) along the axial direction. Next, we calculate individual flux quantities and sum these 66 flux quantities and multiply with 123. This method results in a more accurate calculation of the total magnetic flux, instead of assuming all the wraps have the same magnetic flux and multiplying with the total

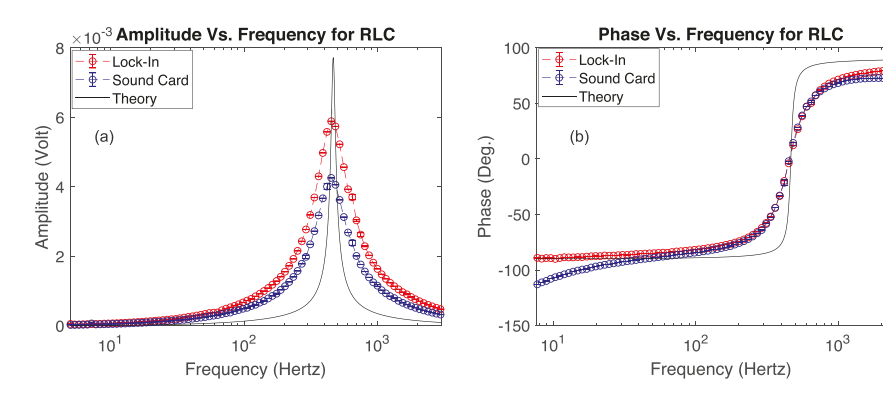


Fig. 3. a) The potential on the resistor as a function of frequency. a) amplitude and b) phase with respect to the input reference. The blue circles (o) and red circles (o) correspond to the soundcard and the lock-in amplifier measurements, respectively. The black line is the theoretical calculation by assuming ideal circuit components.

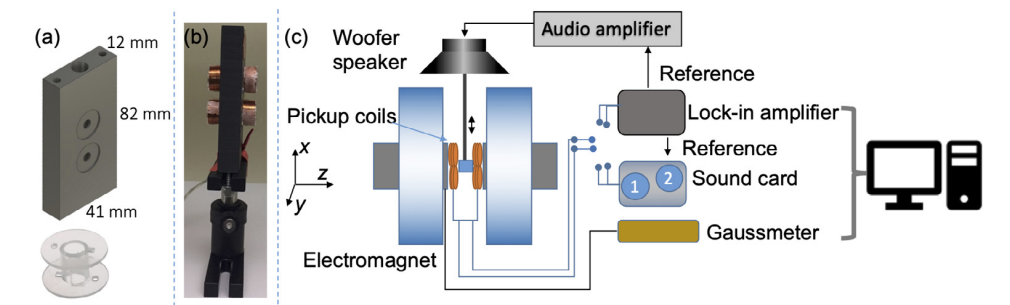


Fig. 4. (a) 3-D printed coil holder with the dimensions of $12 \times 41 \times 82 \text{ mm}^3$. We built the pickup coils from sewing bobbins with a 20 mm diameter and 12 mm width. (b) The picture of pickup coils mounted on 3-D printed holder. (c) Schematic of vibrating sample magnetometer. Four pickup coils are located between the pole pieces of an electromagnet. The sound card and the lock-in amplifier are connected to the VSM turn by turn. A laud woofer speaker and audio amplifier are used to vibrate magnetic samples.

8118 turns.

Next, we find the induced voltage on the coil $V=\frac{d\mathcal{Q}_z}{dt}=\frac{d\mathcal{Q}_z}{dx}\frac{dx}{dt}$, where x is the vibration direction. The displacement of vibration at any time t is represented by $x=Asin\ 2\pi ft$, where f is the frequency and A is the amplitude. Using Mathematica, we first differentiate with respect to x and perform the integration. We finally find the rate of flux change $\frac{d\mathcal{Q}_z}{dx}=36.4\times 10^6Wb/m$ and the induced voltage,

$$V = 4\frac{\mu_0 \times m}{4\pi} (36.4 \times 10^6 \times A2\pi f)$$
 (4)

After we theoretically calculate the induced voltage due to a magnetic moment, we test the sensitivity of our VSM by studying hysteresis curves of three distinct magnetic samples, i.e. a tiny nickel piece (99.99% pure), perm-alloy thin film, and Co/Pt multilayer. The following sections below explicate the theoretical calculations and experimental results obtained in our VSM experiment for each sample.

3.1. Ni piece

In our first test, we use a nickel piece (99.99% pure) with a mass of 0.22 g. Density and the saturation value of magnetization of Ni are given 8.90 g/cm³ and 5.1×10^5 A/m, respectively [1]. The total magnetic moment is found by $m = M \times Volume = 12.75 \times 10^{-3}$ Am². The experiment is repeated for the vibration frequencies of 17 Hz, 34 Hz, and 64.7 Hz and corresponding induced voltages are captured by both the lock-in amplifier and sound card. By using Eq. (4), we find the value of saturated induced voltages $2.38 \times 10^{-2}V$ (with an oscillation amplitude A = 1.22mm), $1.72 \times 10^{-2}V$ (with A = 0.43mm), and $1.92 \times 10^{-2}V$ (with A = 0.26mm), at 17 Hz, 34 Hz, and 64.7 Hz frequencies, respectively. These oscillation amplitudes are found from the displacements of the sample using a high-speed camera.

In the experiment, the time constant and waveform acquisition time for lock-in amplifier and soundcard are maintained at 200 ms and 800 ms, respectively. We also varied the cut off frequency in the Butterworth filter for the optimum mixing of the signals from the sound card. Fig. 5. a), b) and c) represent the measurements of induced

voltages from the Ni piece as the magnetic field sweep from $-0.2\,\mathrm{T}$ to 0.2 T at different frequencies, which are referred to as hysteresis loops. In each plot, blue and red curves represent the soundcard and lock-in amplifier, respectively. The saturation induced voltages measured by the lock-in amplifier are $2.25\times10^{-2}V$, $1.19\times10^{-2}V$, and $2.85\times10^{-2}V$ for the frequencies of 17 Hz, 34 Hz, and 64.7 Hz, respectively. Because the soundcard has complicated filtering and amplification, the measured values with a sound card are calibrated using the lock-in measurements. We note that our experimental results are in very good agreement with the theoretically estimated induced voltages. Moreover, the induced voltage responses measured with the soundcard are in perfect correspondence with the ones obtained with the lock-in amplifier, which illustrates the excellent performance of the soundcard for measuring modulated signals.

3.2. Perm-alloy thin film

As the Ni piece created a large induced signal and provided relatively easy measurements, we next perform a magnetometer on a more challenging perm-alloy thin film sample, which is deposited on a silicon substrate using magnetron sputtering technique. The dimension of the sample is 6 mm \times 7 mm and the thickness of the perm-alloy is 50 nm, which gives the total volume of 21×10^{-13} m³. The magnetization is measured along an easy axis, which is in-plane at this thickness of perm-alloy. Taking the saturation magnetization 800 emu/cm3 of permalloy [23], we find the magnetic moment to be 1.68×10^{-6} Am². The calculated values of saturation induced voltages are $3.26 \times 10^{-6}V$ (with oscillation amplitude A = 2.04mm), $8.29 \times 10^{-6}V$ A = 3.17mm), $1.51 \times 10^{-5}V$ (with A = 2.90mm), and $2.59 \times 10^{-6}V$ (with A = 0.26mm) for the frequencies of 10.4 Hz, 17 Hz, 34.4 Hz, and 64.7 Hz, respectively. The time constant and waveform acquisition time are fixed at 200 ms and 800 ms for the lock-in amplifier and the sound card, respectively.

The hysteresis curves of the film are presented in Fig. 6, and they have a rectangular shape with a small coercive field and an adequate inplane magnetic anisotropy as seen previous perm-alloy thin films

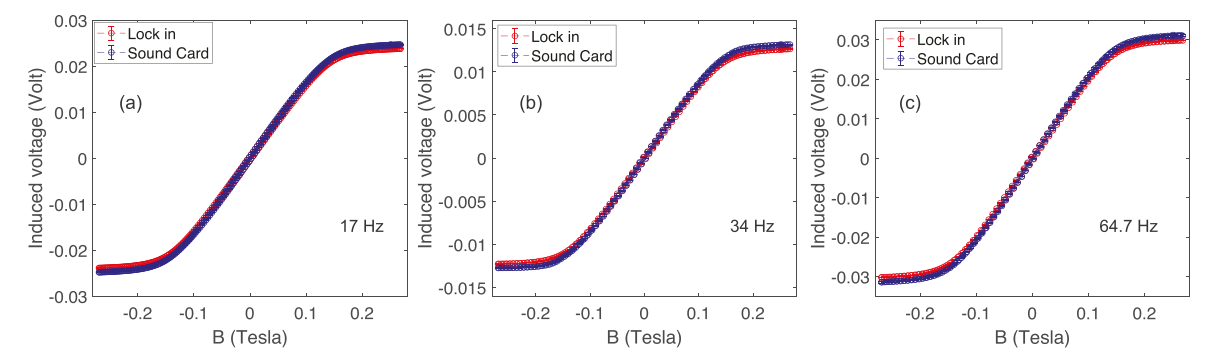


Fig. 5. Induced voltages as a function of an applied magnetic field (B) at a) 17 Hz, b) 34 Hz, c) 64.7 Hz frequencies. The red and blue curves represent the hysteresis measurements with the lock-in amplifier and the sound card, respectively.

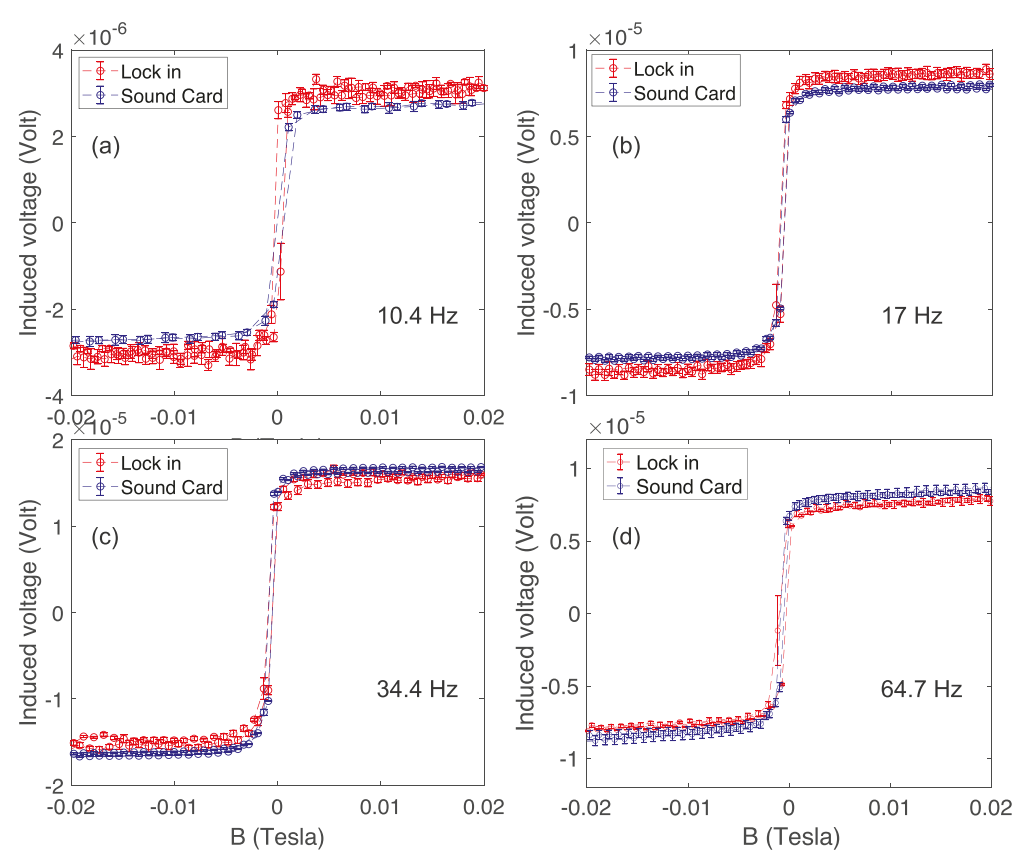


Fig. 6. The hysteresis loops of a perm-alloy thin film with an easy plane anisotropy. The red data points represent the measurements with the lock-in amplifier and the blue points are for the sound card-measurements at (a) 10.4 Hz (b) 17 Hz, (c) 34.4 Hz and, (d) 64.7 Hz vibration frequencies.

[23,24]. A linear background of the hysteresis curve is subtracted due to the diamagnetic nature of the silicon substrate [25]. In all frequencies, the measurements of the sound card have a complete overlap with that of the lock-in amplifier. Furthermore, at lower frequencies, the sound card data are still smoother than that of the lock-in amplifier, even though the signal is reduced due to the filtering in the sound card, which can be taking account as a calibration factor. The values of saturation induced voltages are $2.82 \times 10^{-6}V$, $8.33 \times 10^{-6}V$, $1.47 \times 10^{-5}V$, and $8.18 \times 10^{-6}V$ at the frequencies of 10.4 Hz, 17 Hz, 34.4 Hz, and 64.7 Hz, respectively. For all the frequencies except 64.7 Hz, we have very good agreement with the calculated induced voltage. For 64.7 Hz, our measurement of vibration amplitude may have a large error.

Although the Ni-bulk piece with lower vibration amplitudes gave a comparable signal for all the frequencies, we tried to increase the vibration amplitude for the Perm-alloy film at 64.7 Hz and obtained worse hysteresis curves. The reason behind this performance drop is that the loudspeaker (vibrator) becomes hot above 60 Hz frequencies and causes a decrease in the vibration amplitude and results in inconsistent measurements. In our VSM design, by choosing a loudspeaker as the vibrator, we significantly decrease the cost, but we have to limit our vibration frequencies below 60 Hz. A superior vibrator can increase the performance of VSM when the frequency is used above 60 Hz to avoid noises from the AC (outlet) lines.

3.3. Co/Pt multilayers with perpendicular magnetic anisotropy

As the last sample, we grew a magnetic multilayer with a perpendicularly aligned magnetic anisotropy. On a Si substrate, we deposited Ta(4 nm)/[Co(0.4 nm)/Pt(0.4 nm)] $_{\rm x3}$ /Pt(3 nm) multilayer using sputtering technique. This Co/Pt multilayer has been reported to have a perpendicular magnetic anisotropy and there is a great interest in such

multilayer films for spintronics applications with topological spin textures [26–32]. The dimension of the sample is 6 mm \times 8.5 mm and the total thickness of the magnetic material is 1.2 nm. We use the saturation magnetization of Cobalt1.4 \times 10⁶A/m [1 29] and find the expected magnetic moment to be 8.6 \times 10⁻⁸ Am^2 . The respective calculated induced voltages at the frequencies of 17.4 Hz and 34.7 Hz are 4.33 \times 10⁻⁷V (with A=3.17mm) and 3.30 \times 10⁻⁷V (with A=1.2mm). We increased the driving voltage on the laud speaker for a larger displacement about 20%. From the perm-alloy hysteresis, we found these two frequencies give the highest signals, therefore, we measured only at these two frequencies for the Co/Pt multilayer sample.

In the experiment, the sample is aligned perpendicular to the direction of the applied field, which makes the easy axis along the field direction. The time constant and acquisition time for the signal detection are set at 1 and 6 s, respectively, for the lock-in amplifier. Whereas, for the SC, the corresponding values are set at 1 and 2.8 s. The magnetizations observed in two distinct frequencies clearly illustrate a perpendicular magnetic anisotropy for Co/Pt multilayer. As plotted in Fig. 7, our hysteresis curves have a rectangular shape and agree with the previous measurements on similar multilayer samples [32]. We obtained saturation induced voltages of $4.14 \times 10^{-7}V$ and $3.28 \times 10^{-7}V$ for the frequencies of 17.4 Hz and 34.7 Hz, respectively. These voltages are in close agreement with those values obtained from the theoretical calculation of induced voltage. The proximity between the data sets of lock-in and sound-card shows the promise of a soundcard for such characterization. Especially, we note that perpendicular magnetic anisotropy films are relatively challenging samples for VSM characterization due to being very thin.

To confirm the coercivity field and perpendicular magnetic anisotropy of Co/Pt multilayer, we performed an Anomalous Hall effect measurement of the film. As shown in Fig. 7c, we have a perfect

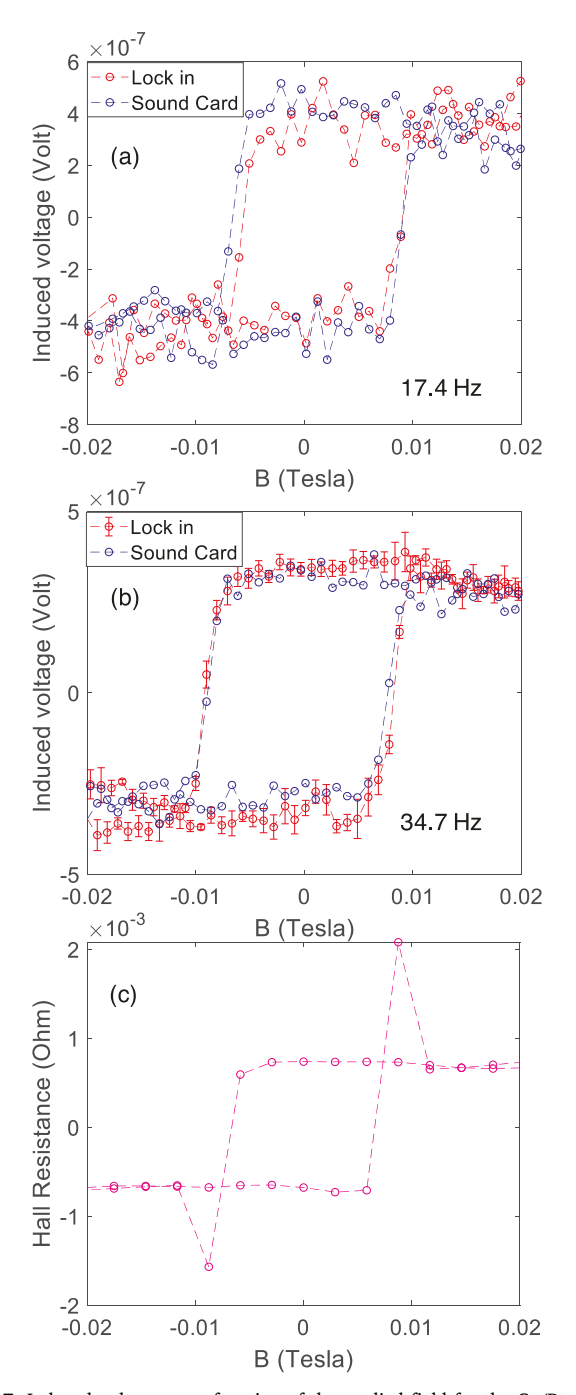


Fig. 7. Induced voltages as a function of the applied field for the Co/Pt multilayer sample from the lock-in amplifier (red) and soundcard (blue) at (a) 17.4 Hz, (b) 34.7 Hz frequencies. (c) Hall effect measurement of the same film. Anomalous Hall effect shows the same coercivity field as in (a) and (b).

agreement with the VSM measurements, which is strengthening the reliability of our audio-based VSM experiment.

4. Discussion and summary

In summary, we developed a low-cost but sensitive and versatile magnetometry instrument based on audio components, including a sound card, amplifier, and laud speaker. We first tested the frequency responses of the LCR series circuit by using both the sound card and a commercial lock-in amplifier. This circuit test verified the frequency

range of our sound card that can reliably measure a modulated signal. Next, we built a sensitive 4-coil VSM by utilizing the sound card and induced voltages were theoretically calculated for its coil geometry. We then measured the magnetization hysteresis curves of a Nickel piece, a 50-nm-thick Perm-alloy film, and a perpendicularly magnetized Co/Pt multilayer samples using the sound card and the lock-in amplifier. Two data sets obtained from two instruments had a perfect agreement. In addition, we confirmed the hysteresis curve of Co/Pt multilayer film with the Hall effect measurement. The noise of our sound-card based VSM is approximately 5.4×10^{-6} emu, which is obtained by vibrating the sample holder without any magnetic sample. With a similar configuration, the noise of VSM with the commercial lock-in amplifier, however, is 3.8×10^{-5} emu at 34.7 Hz. When the Co/Pt multilayer sample is inserted, the RMS value of the noise is 2×10^{-6} emu with the sound card and 1×10^{-5} emu with the lock-in amplifier. Although sound cards are not calibrated as an off-shelf scientific measurement unit, their high bit ADC and fast sampling rates can be exploited for measuring modulated signals, such as in VSM measurements, at a very low cost after calibrating with a lock-in amplifier or other means.

Declaration of Competing Interest

The authors declare that they have no known competing financial interests or personal relationships that could have appeared to influence the work reported in this paper.

Acknowledgement

This work was supported by the National Science Foundation grant number OIA-1929086.

Appendix A. Supplementary data

Supplementary data to this article can be found online at https://doi.org/10.1016/j.jmmm.2020.166560.

References

- [1] M. Getzlaff, Fundamentals of Magnetism, Springer, New York, NY USA, 2008 doi: 10.1007/978-3-540-31152-2.
- [2] S. Foner, The vibrating sample magnetometer: experiences of a volunteer (invited), J. Appl. Phys. 79 (1996) 4740, https://doi.org/10.1063/1.361657.
- [3] H.J. Richter, An analysis of magnetization processes in metal evaporated tape, IEEE Trans. Magn. 29 (1993) 21–33, https://doi.org/10.1109/20.195545.
- [4] E. Joven, A. del Moral, J.I. Arnaudas, Magnetometer for anisotropy measurement using perpendicular magnetization, J. Magn. Magn. Mater. 83 (1990) 548–550, https://doi.org/10.1016/0304-8853(90)90620-6.
- [5] N. Matsubara, F. Sai, Measurement of magnetization on an obliquely deposited film by using 3-dimensional vector VSM, IEEE Trans. Magn. 27 (1991) 4748–4750, https://doi.org/10.1109/20.278935.
- [6] H.J. Richter, H. Hibst, Vectorial magnetization of metal evaporated tapes, J. Appl. Phys. 70 (1991) 5512, https://doi.org/10.1063/1.350208.
- [7] R.L. Fagaly, Superconducting quantum interference device instruments and applications, Rev. Sci. Instrum. 77 (2006), https://doi.org/10.1063/1.2354545.
- [8] S. Legl, C. Pfleiderer, K. Krämer, Vibrating coil magnetometer for milli-Kelvin temperatures, Rev. Sci. Instrum. 81 (2010) 79–82, https://doi.org/10.1063/1. 3374557.
- [9] S.A.H. Shah, Vibrating Sample Magnetometery: Analysis and Construction, Thesis. (2013).
- [10] Magnetometry, Aim: Magnetic characterization of ferromagnetic samples by Vibrating Sample, (2016).
- [11] T. John, D. Pietschmann, V. Becker, C. Wagner, Deconvolution of time series in the laboratory, Am. J. Phys. 84 (2016), https://doi.org/10.1119/1.4960294.
- [12] A.K.D. Gopman, D. Bedau, A digitally configurable measurement platform using audio cards for high-resolution electronic transport studies, Rev. Sci. Instrum. 83 (2012), https://doi.org/10.1063/1.4709498.
- [13] J. Sinlapanuntakul, P. Kijamnajsuk, C. Jetjamnong, S. Chotikaprakhan, Digital lockin amplifier based on soundcard interface for physics laboratory, J. Phys. Conf. Ser. (2017), https://doi.org/10.1088/1742-6596/901/1/012065.
- [14] J. Mathews, R.L. Walker, Mathematical Methods of Physics, second ed., Addison-Wesley, New York, NY, 1971.
- [15] J. Mallinson, Magnetometer coils and reciprocity, J. Appl. Phys. 37 (1966) 2514–2515, https://doi.org/10.1063/1.1708848.
- [16] J. Bernards, Design of a detection coil system for a biaxial vibrating sample

- magnetometer and some applications, Rev. Sci. Instrum. 64 (1993) 1918–1930, https://doi.org/10.1063/1.1143977.
- [17] S. Foner, Versatile and sensitive vibrating-sample magnetometer, Rev. Sci. Instrum. 30 (1959) 548, https://doi.org/10.1063/1.1716679.
- [18] A. Zieba, S. Foner, Detection coil, sensitivity function, and sample geometry effects for vibrating sample magnetometers, Rev. Sci. Instrum. 53 (1982) 1344–1354, https://doi.org/10.1063/1.1137182.
- [19] T.M. El-Alaily, M.K. El-Nimr, S.A. Saafan, M.M. Kamel, T.M. Meaz, S.T. Assar, Construction and calibration of a low cost and fully automated vibrating sample magnetometer, J. Magn. Magn. Mater. 386 (2015) 25–30, https://doi.org/10.1016/ j.jmmm.2015.03.051.
- [20] N. Hosseini, S. Khiabani, F. Sarreshtedari, M. Fardmanesh, Optimized design and implementation of low-cost, sensitive and versatile vibrating sample magnetometer, ICEE 2012–20th Iran, Conf. Electr. Eng. (2012) 202–205, https://doi.org/10.1109/ Iranjan/CFE 2012 6392353.
- [21] W. Burgei, M.J. Pechan, H. Jaeger, A simple vibrating sample magnetometer for use in a materials physics course, Am. J. Phys. 71 (2003) 825–828, https://doi.org/10. 1119/1.1572149.
- [22] J.A. Gerber, W.L. Burmester, D.J. Sellmyer, J.A. Gerber, W.L. Burmester, D.J. Sellmyer, Simple vibrating sample magnetometer, Rev. Sci. Instrum. 53 (2013) 691, https://doi.org/10.1063/1.1137043.
- [23] D. Jordán, D. González-Chávez, D. Laura, L.M. León Hilario, E. Monteblanco, A. Gutarra, L. Avilés-Félix, Detection of magnetic moment in thin films with a home-made vibrating sample magnetometer, J. Magn. Magn. Mater. 456 (2018) 56–61, https://doi.org/10.1016/j.jmmm.2018.01.088.
- [24] D. Mauri, D. Scholl, H.C. Siegmann, E. Kay, Magnetism in very thin films of permalloy measured by spin polarized cascade electrons, Appl. Phys. A Solids Surf. 49

- (1989) 439-447, https://doi.org/10.1007/BF00617010.
- [25] K.Q. Lin, L. Sen Wang, Z.W. Wang, R.T. Wen, Y. Chen, D.L. Peng, Gas-phase synthesis and magnetism of HfO2nanoclusters, Eur. Phys. J. D. 67 (42) (2013), https://doi.org/10.1140/epjd/e2013-30524-9.
- [26] W. Jiang, P. Upadhyaya, W. Zhang, G. Yu, M.B. Jungfleisch, F.Y. Fradin, J.E. Pearson, Y. Tserkovnyak, K.L. Wang, O. Heinonen, S.G.E. Te Velthuis, A. Hoffmann, Blowing magnetic skyrmion bubbles, Science (80) 349 (2015) 283–286, https://doi.org/10.1126/science.aaa1442.
- [27] S. Emori, U. Bauer, S.M. Ahn, E. Martinez, G.S.D. Beach, Current-driven dynamics of chiral ferromagnetic domain walls, Nat. Mater. 12 (2013) 611–616, https://doi. org/10.1038/nmat3675.
- [28] A. Fert, N. Reyren, V. Cros, Advances in the physics of magnetic skyrmions and perspective for technology, Nat. Mater. 2 (2017) 17031, https://doi.org/10.1038/ natreymats 2017 31
- [29] V.A. Bautin, A.G. Seferyan, M.S. Nesmeyanov, N.A. Usov, Magnetic properties of polycrystalline cobalt nanoparticles, AIP Adv. 7 (2017) 045103, https://doi.org/ 10.1063/1.4979889.
- [30] R. Shan, T.R. Gao, S.M. Zhou, X.S. Wu, Y.K. Fang, B.S. Han, Co/Pt multilayers with large coercivity and small grains, J. Appl. Phys. 99 (2006) 063907, https://doi. org/10.1063/1.2184435.
- [31] B. Zhang, K.M. Krishnan, C.H. Lee, R.F.C. Farrow, Magnetic anisotropy and lattice strain in Co/Pt multilayers, J. Appl. Phys. 73 (1993) 6198–6200, https://doi.org/ 10.1063/1.352696.
- [32] J.H. Park, C. Park, T. Jeong, M.T. Moneck, N.T. Nufer, J.G. Zhu, CoPt multilayer based magnetic tunnel junctions using perpendicular magnetic anisotropy, J. Appl. Phys. 103 (2008) 07A917, https://doi.org/10.1063/1.2838754.